Wave Kinematics on Breakwater Heads and Stability of Armour Layers under Multidirectional Waves

Yoshiharu Matsumi [1], Akira Kimura [2] and Kenichi Ohno [3]

Abstract

This study complements the wave kinematical investigation on the performance of rubble mound breakwater under uni and multidirectional waves. The measurements of wave kinematics over the head and trunk sections were undertaken to achieve an improved understanding of the influence of wave directionality on the stability of armour layers. The directionality and magnitude of velocity vectors over the head and trunk sections under 3D waves were assessed by comparing them with the measurements under 2D waves. The sensitive zones of the initial damage in the head and trunk were evaluated by linking the velocity measurements with the stability formulas for armour stone movement.

Introduction

Recently there have been studies published, which have examined breakwater stability under uni and multidirectional waves. Unfortunately those studies still may not have established trends for whether or not the influence of wave directionality in multidirectional seas leads to more loads on the breakwater. The staple reason of limited understanding is that the characteristics of the structure such as the slope, the type of armour layer and the breakwater geometry may contribute to different types of breakwater damage. Therefore, a better approach to achieving a comprehensive understanding of the influence of multidirectional waves on breakwater stability is to make the kinematics of the various multidirectional waves over the breakwater, which are concerned in the damage, clear.

In our previous experimental study (1996), the spatial characteristics in correlation of the magnitude of measured velocity vectors over the head were

1 Associate Professor, D. Eng., Dept. of Social Systems Eng., Tottori University, Tottori 680-8552, Japan.
2 M. ASCE, Professor, D. Eng., Dept. of Social Systems Eng., Tottori University
3 Graduate Student, M. Eng., Dept. of Social Systems Eng., Tottori University

investigated. In the case of multidirectional waves, the correlation in the middle and back head was very poor regardless of the mean direction of waves and peak periods. From those results, possibility of oblique wave attacking directly the heads due to the directional spread in multidirectional seas could be supported. When relating the initial damage in the head and trunk sections to those oblique waves in the multidirectional seas, those direct wave attacks may lead to higher loads on the armour stones at some local position in the head and trunk. Namely, the location of the sensitive zones where the initial damage occurred under multidirectional waves is deemed to be stronger than the case of unidirectional waves.

The main objective of the present study is to compare wave kinematics under the effect of uni and multidirectional waves in terms of measured magnitudes and directions of velocity vectors over the breakwater. Furthermore, the direct unexpected oblique wave attacks, which are associated with the directional spread of multidirectional waves may cause more damage to the armour layers at some local position in the breakwater. Therefore, the difference in the sensitive damage zones under 2D and 3D waves is also evaluated by linking the velocity measurements with the stability formula for armour stone movement on the slope, which was proposed by authors (1996).

Experimental Setup

Layout of breakwater model

Physical model tests were carried out, at the Tottori University, in the multidirectional wave basin that had a length of 14m and a width of 8.4m. Figure 1 shows a plan view of the experimental setup. A fourteen-segment snake generator is located along one of the 8.4m sides of the basin. Expanded polystyrene absorbers with permeability, capable of limiting wave reflections to 20% for most frequencies of interest, are installed along the two sides of the basin. The slope of 1:5 and 1:30 is placed on the side opposite the wave generator, in order to ensure an efficient dissipation of wave energy.

The layout of the breakwater model had to be designed carefully to ensure homogeneous sea states on the breakwater. For this purpose, the numerical model (Isaacson; 1992) which was based on the diffraction theory and used the boundary integral equation was adopted in this study. This model can predict the water surface elevation and kinematics of the sea states prevailing at different locations in the basin. A sample output resulting from this numerical model is shown in Figure 2. It illustrates the spatial distribution of wave heights under a multidirectional sea state (mean angle of incidence (α); $\alpha=0^\circ$) in the basin without the breakwater model in place. The expected wave heights presented in this figure were normalized with respect to the target wave height. The useful test area, over which the sea state is homogeneous, is limited by a triangular boundary. According to this figure, the best location for the model would be close to the paddle. However, since this wave basin was not yet equipped with active absorption, in order to minimize re-reflections from

the paddles, the model was placed with its longitudinal axis rotated 20 ° with respect to the paddles, as shown in Figure 1.

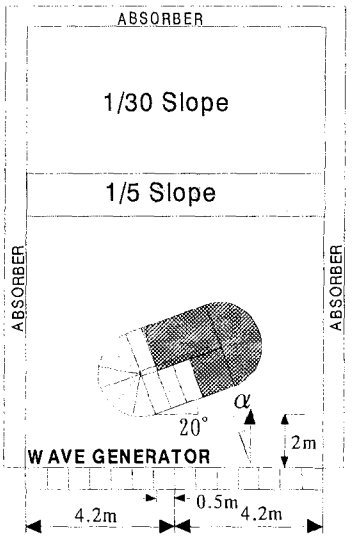

Figure 1 Plan view of the experimental setup.

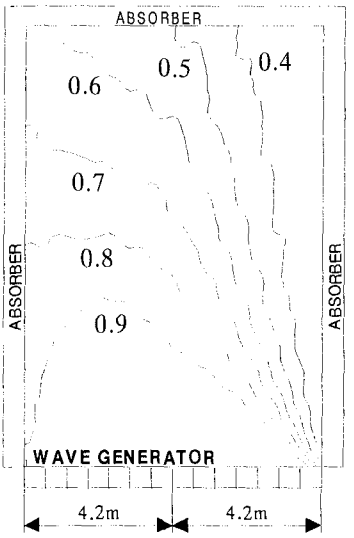

Figure 2 Spatial distribution of wave heights in the basin without the model.

Breakwater model

Figure 3 shows both plan and profile views of the breakwater model adopted in this study. The three dimensional rubble-mound breakwater consisted of two outer layers of armour stones and a relatively porous core, and was built with a slope of 1:2. Its height was 50cm and it performed as a non-overtopping structure in a water depth of 30cm, which was adopted in this experiment. Since the purpose of this study was to investigate the wave velocity field over the head and trunk sections without any damage, the whole surface of the breakwater was covered with a hard nylon mesh in order to restrain the armour stones. The reflection characteristics of the breakwater were estimated under unidirectional waves of normal incidence in the preliminary experiments. The resulting reflection coefficient was about 25%.

The characteristics of the armour and core stones used in this study are presented in Table 1. The weight of armour stones, W_{50}, was 42 gf, this value was 1.5 times the weight estimated by Van der Meer's formula (1987) with damage

parameter S=2 against the targeted significant wave height, H_{m0}=6cm, and peak wave period, Tp=1.4s. The gradations of the armour stones were meticulously checked and the resulting D_{n85}/D_{n15} ratio for the armour was 1.1.

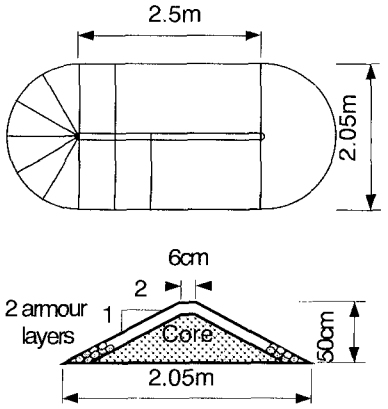

Figure 3 Plan and profile view of the breakwater model.

Table 1 Summary of the breakwater characteristics.

W_{50} weight of armour	42gf
W_{a50} weight of core	3.75gf
D_{n50} nominal diameter of armour	2.51cm
Porosity of armour layers	0.45
D_L Length of head	205cm
T_L Length of trunk	250cm
Crest breadth	6cm
Height of breakwater	50cm

$D_{n50}=(W_{50}/\rho_s)^{1/3}$

ρ_s : unit weight of armour stone

Layout of current meters and wave gauges

The velocity field over the head and trunk sections was measured using 6 bi-axial electromagnetic current meters at 124 different locations indicated by dotes in Figure 4. The measuring points in the head sections were located at 10° intervals from the top of front head in a clockwise direction (θp). In the trunk section, these points are located at 10cm intervals. The water surface elevations of the sea states in the proximity of the model were measured using 8 wave gauges at 8 different locations indicated by circles in Figure 4.

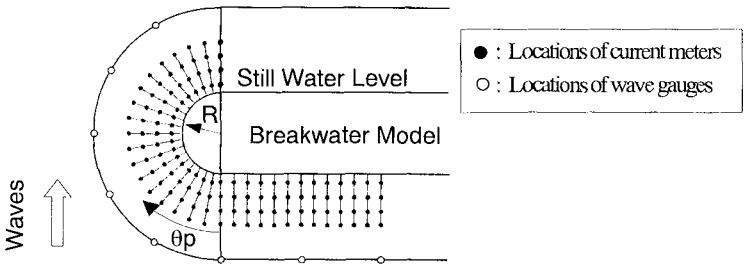

Figure 4 Measuring points of velocity components over the breakwater.

Test series

Table 2 indicates the characteristics of the incident waves adopted in these experiments. The spectra were the JONSWAP type with two different peak periods (Tp=1.0s, 1.4s). The peak enhancement factor (γ) was chosen to be equal to 3.3. The multidirectional waves were simulated by using the well-known Single Summation Method. For the directional spreading function, the Mitsuyasu-type (1975) was chosen, the spreading parameter (s) was given by the following form (Goda 1985):

$$s = \begin{cases} S_{max} \cdot (f/f_p)^5 & : f \le f_p \\ S_{max} \cdot (f/f_p)^{-2.5} & : f \ge f_p \end{cases}$$

Here f_p denotes the frequency at the spectral peak. Values of S_{max}=5 and $S_{max} = \infty$ were applied to simulate multi and unidirectional waves respectively. In order to assess the influence of obliqueness, two different mean angles of incidence α=0° and α=−15° were used, ensuring at the same time homogeneity of the sea state at the head and trunk sections.

In order to minimize statistical variability associated with short wave record lengths, a recycling period (T_R) of 20 minutes in model scale was used in the synthesis. This storm duration corresponded to about 1400 waves when Tp=1.0s and about 1000 for Tp=1.4s. The ratios of diameter of the head (D_L) over wave length and length of trunk (T_L) over wave length are indicated in Table 2. In each test series, the sea states were pre-calibrated in the basin without the structure in position, while keeping all wave gauges in place. The water depth was 30cm uniformity.

Table 2 Characteristics of incident waves in experiments.

Spectrum	Tp (s)	γ	Hm0 (cm)	α (deg.)	Smax	T_R (min.)	N	D_L/L	T_L/L
JONSWAP	1.0	3.3	6, 8.5	0, -15	5,∞	20	1440	1.49	1.82
JONSWAP	1.4	3.3	6, 8.5	0, -15	5,∞	20	1028	0.95	1.16

Directional Distribution of Velocity Vectors over the Head

This study has discussed the velocity vectors, which pass a magnitude above the highest 1/10 of those magnitudes evaluated from time series data of the velocity measurements. Because, the armour stones of breakwater may be strongly prone to move under conditions of faster flow velocities.

Figures 5(a)-(d) show examples of the distribution of the relative

frequencies in directionality of the individual velocity vectors in the time series data of the measurements at four difference positions in the head section for uni ($S_{max}=\infty$) and multidirectional waves ($S_{max}=5$) under normal incidence. Line of 180-0 in every figure is normal to the trunk, bold solid lines (ex. line 60-240 in figure (a)) indicate a line tangent to the horizontal curve of the head at four positions respectively, as shown in figure (e).

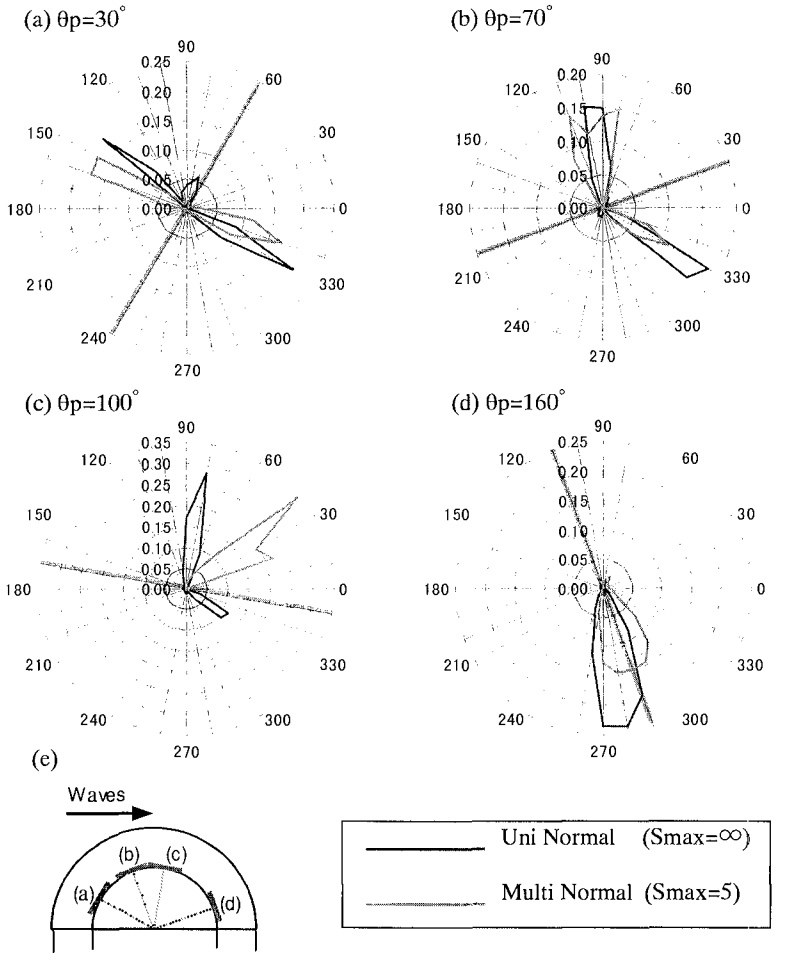

Figure 5 Distribution of directionality of velocity vectors over the head.

From these figures, the directionality of the velocity vectors under 3D waves is wider than that under 2D waves due to the directional spreading of waves. In figures (a) and (b), the characteristics of the velocity field from the front head section to the top of middle head section are mainly dominated by flow of the runup and rundown of waves on the slope. The center of middle section as seen in figure (c), demonstrates the flow towards down-slop of the head. And the prevailing direction of velocity vectors under 3D waves is different from that of 2D waves. This phenomenon may be generated by reflected waves, which are generated by the oblique wave attacks due to directional spread of 3D waves. In the back head section of figure (d), the flow towards the rear surface of breakwater only exists under both 3D and 2D waves. The difference in the direction of velocity vectors over the head section under 2D and 3D waves remarkably occurs in middle head section by the directional spread of 3D waves. Therefore, in the next section, the influence of this difference on the stability of head and trunk is investigated by linking the stability formulas for armour stones with the measurements of velocity over the breakwater.

Stability of Armour Stones in Head and Trunk

In this section, the sensitive zones of the initial damage in the head and trunk sections will be evaluated by linking the velocity measurements with the stability formulas for armour stone movement. These formulas have been derived by taking account of tangential slope of the breakwater with respect to the direction of velocity vectors.

(a) Case of Head (b) Case of Trunk

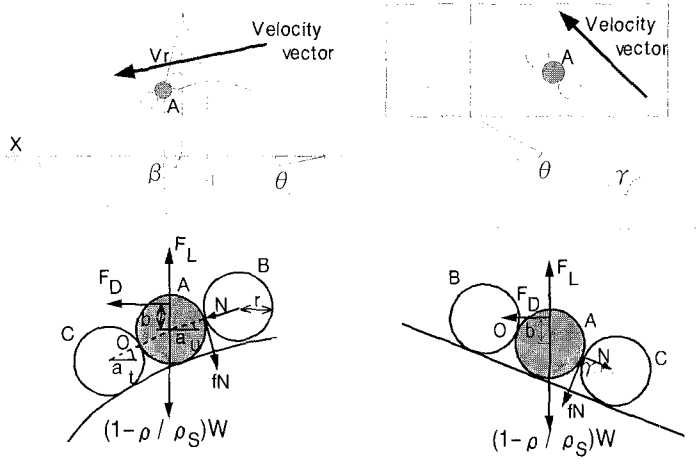

Figure 6 Attacking velocity and hydrodynamics forces on armour stone in head and trunk.

Critical velocity for stability of armour stones in head and trunk

In Figure 6(a), the armour sphere (A) is placed on the head with the horizontal angle (β) for the velocity vector (V_r) with horizontal angle (θ). By assuming the shape of the head is a circular cone, the curve of intersection between the vertical plane and the cone becomes a hyperbola. In this study, the both drag and lift forces were considered as hydrodynamic forces acting on the armour stones. Then, the equilibrium equations between the armour weight and the hydrodynamic forces can be derived by balancing the moment about point O in these figures:

(a) Case of Head

$$\left(1-\frac{\rho}{\rho_S}\right)W[\cos a_t + f\sin a_u\{1+\cos(a_t - a_u)\}] = F_D\left(\sin a_t + \frac{b}{r}\right) + F_L\cos a_t \qquad (1)$$

(b) Case of Trunk

$$\left(1-\frac{\rho}{\rho_S}\right)W[\cos\gamma + 2f\sin\gamma] = F_D\left(-\sin\gamma + \frac{b}{r}\right) + F_L\cos\gamma \qquad (2)$$

where W and r are weight and diameter of armour stone, ρ_s and ρ are unit weight of stone and water, F_D and F_L are drag and lift forces, f is friction coefficient between stones, b is distance between the center of stone and drag force acting point. The parameters a_u and a_t in Eq. (1) are respectively the angle of elevation of armour sphere (A) from (C), and (B) from (A) as shown in Figure 6(a). The parameter γ in Eq. (2) is the angle of slope of the trunk section against the attacking velocity vector as shown in Figure 6(b). In this study, the drag and lift forces are described by the following formulas, respectively:

$$F_D = m'\rho\pi r^2 V_r^2 \qquad (3)$$

$$F_L = \frac{1}{2}\varepsilon C_L\rho\pi r^2 V_r^2 \qquad (4)$$

where m' and C_L are drag and lift coefficients respectively, ε is sheltering coefficient of armour stone against the velocity. In Eqs. (1)-(4), f, m', C_L, ε and b are unknown parameters, a_u, a_t and γ can be derived from tangential slope of the breakwater with respect to the velocity vector. Assuming that a_t is equal to a_u for simplicity in this study, they are given by following equation after the simple mathematical analysis.

$$a_t = a_u = \tan^{-1}\left\{\frac{1}{2}\cos(\beta-\theta)\right\} \qquad (5)$$

$$\gamma = \tan^{-1}\left(\frac{1}{2}\cos\theta\right) \tag{6}$$

Finally, the critical velocities (V_{rcH}, V_{rcT}) for armour stone movement in the head and trunk sections are respectively expressed as:

$$\frac{V_{rcH}^2}{gr} = \frac{\left(1-\frac{\rho}{\rho_S}\right)\{1 \pm f\cos(\beta-\theta)\}}{\frac{3}{4}\frac{\rho}{\rho_S}\left[m'\left\{\frac{\cos(\beta-\theta)}{2}+\frac{b}{r}\sqrt{1+\left\{\frac{\cos(\beta-\theta)}{2}\right\}^2}\right\}+\frac{\varepsilon C_L}{2}\right]} \tag{7}$$

$$\frac{V_{rcT}^2}{gr} = \frac{\left(1-\frac{\rho}{\rho_S}\right)(1 \mp f\cos\theta)}{\frac{3}{4}\frac{\rho}{\rho_S}\left[m'\left\{-\frac{\cos\theta}{2}+\frac{b}{r}\sqrt{1+\left(\frac{\cos\theta}{2}\right)^2}\right\}+\frac{\varepsilon C_L}{2}\right]} \tag{8}$$

When the tangential slope with respect to attacking velocity vector becomes positive, in Eqs. (7) and (8), the plus and minus sign before the friction coefficient are replaced by minus and plus sign, respectively. The unknown parameters m', C_L, b, f and ε in Eqs. (7) and (8) were considered as m'=1, C_L=0.5, b=0.5r, f=0.4 and ε=0.4 for simplicity in this paper.

Influence of wave directionality on sensitive zones for damage

In order to investigate the influence of the aforementioned difference in the directional spread of the velocity vectors under 2D and 3D waves on the stability of breakwater head and trunk, the spatial occurrence frequencies for armour stone movement in the head and trunk sections are estimated by linking Eqs. (7), (8) and the velocity vectors which have been measured at 124 points shown in Figure 4.

Figures 7(a) and (b) show the spatial distribution of the calculated occurrence frequencies for armour stone movement in the head and trunk sections under normal 3D and 2D waves conditions, where Tp=1.4s and H_{m0}=6cm. R is the distance in the radial direction from the center of head as shown in Figure 4. In these figures, the contour lines of relative occurrence frequencies which are normalized with respect to the total number of velocities measured for 20 minutes, are indicated with interval every 0.004.

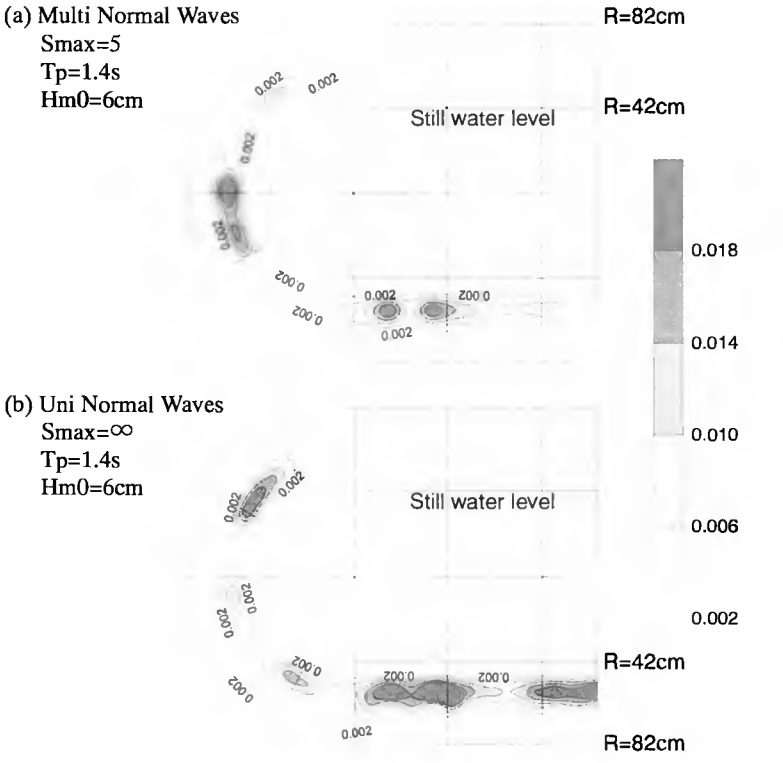

Figure 7 Spatial distributions of occurrence frequencies for armour stone movements.

It can be found that the sensitive zones for armour stone movement in the head section appear typically at three locations; the front, middle and back head sections, respectively. There is obviously a difference between the values of both occurrence frequencies under 3D and 2D waves. Namely, under unidirectional waves (Figure 7(b)), a more sensitive zone for armour stone movement appears in the back head section. Under unidirectional waves attack, it could be observed in the damage tests (Matsumi et al, 1994) that the damage in the back head section was caused to plunge of the strong current with the high velocities generated by the refraction, shoaling and diffraction processes. On the other hand, under multidirectional waves (Figure 7(a)), the middle section is more sensitive parts for the initial damage. The reason for this phenomenon may be the oblique waves directly attacking that section due to the directional spread associated with the multidirectional seas, which have been mentioned in the direction of velocity vectors (Figure 5(c)). For the trunk

section, the sensitive zone for armour stone movements under 2D waves appears at the whole section. In the case of 3D waves, the existence of the oblique waves has resulted in remarkable spot sensitive zone.

Under oblique incidence, the sensitive zones for armour stone movement in the case of 2D waves were shifted to the rear direction of breakwater with near angle of incidence. In the case of 3D waves, there is no difference between the locations of sensitive zones under normal and oblique incidence, as shown in Figure 8. The reasons for it are unclear, but are possibly due to the wide directional spreading value (Smax=5) adopted in this study.

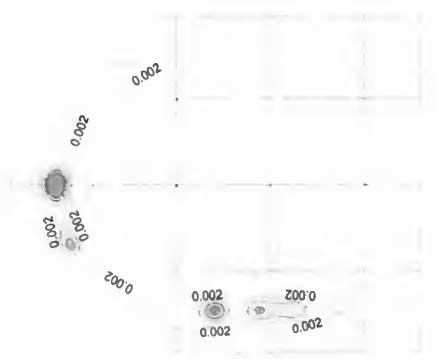

Figure 8 Spatial distributions of occurrence frequencies for armour stone movements under oblique 3D waves (Smax=5, Tp=1.4s, Hm0=6cm, α=-15°).

In order to investigate the reliability of these calculations, initial damage tests of armour stones in the head and trunk sections were carried out under the same incident wave conditions as those in the velocity measuring tests. It can be presumed that the repeatability in the damage tests is not good, because the interlocking force of individual stones placed on the breakwater model may be different in every testing case. Then, in this study, the damage tests under the same wave condition were repeated five times. The resulting initial damage zones where the second armour layer was clearly exposed due to the displacement of the first armour layer under 3D and 2D waves attack are shown in Figures 9(a) and 9(b), respectively. The damage areas shown in these figures indicate parts where the initial damage in the same position on the breakwater occurred more than three times in five tests. By comparing these initial damage patterns with the spatial distributions of occurrence frequencies for armour stone movements shown in Figure 7, it can be seen that the calculated results of the sensitive zones for damage of stones in the head and trunk sections are fairly close to the experimental locations.

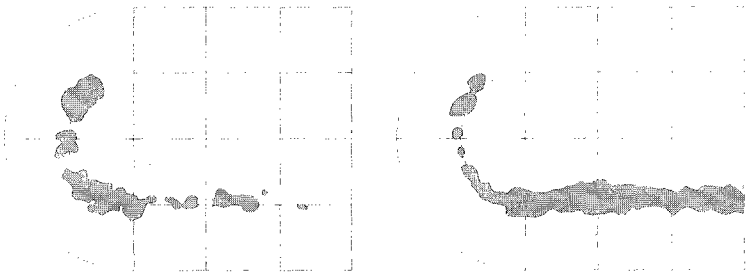

(a) Multi Normal Waves (Smax=5) (b) Uni Normal Waves (Smax=∞)

Figure 9 Initial damage zones in the experiments.

Magnitude of velocities over head

Figures 10(a) and 10(b) show the spatial distribution of occurrence frequencies for velocities (V_r) beyond the critical velocity (V_{rcH}) at the head section. The contour lines of relative occurrence frequencies are normalized with respect to the total number of velocities measured in 20 minutes.

In the case of 3D waves (Figure 10(a)), the maximum magnitude of velocities acting on the middle head section becomes nearly 3.5 times the value of critical velocity. This phenomenon may be pointed out to depend on the direct oblique wave attacks, which are associated with the directional spread of 3D waves. On the other hand, in the case of 2D waves, the high velocities with higher occurrence frequencies than those of 3D waves appear especially in the back head section. It has been observed in the damage tests that the reason for it depends on plunge of the strong current generated by refraction, shoaling and diffraction processes on the front and middle head sections

Conclusion

The prevailing velocity vectors in the middle head section under 3D waves flow towards the down-slop of the head. This occurrence may be generated by the reflected waves which are produced by the oblique waves directly attacking the front head section.

The presented equations of the critical velocity for armour stone movement in the head and trunk sections could satisfactorily explain the initial damage zones in the damage tests. The middle head section under 3D waves is the most sensitive zone for the initial damage. Under 2D waves, a more sensitive zone appears in back head section. For the trunk section, the sensitive zone for the initial damage under 2D

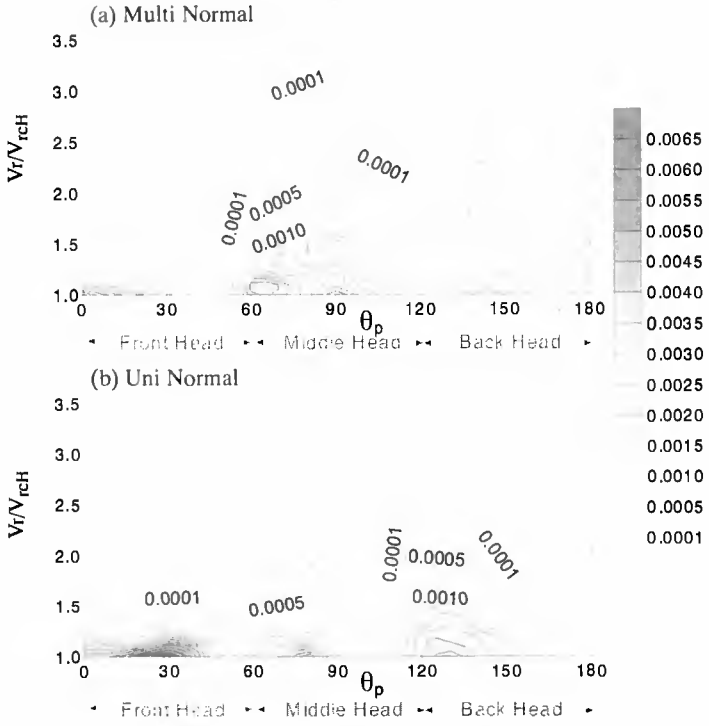

Figure 10 Spatial distribution of occurrence frequencies for velocities beyond critical velocity (V_{rcH}).

waves appears at the whole section. In the case of 3D waves, the sensitive damage zones become spot patterns because of the existence of the oblique waves.

The maximum magnitude of velocities acting on the middle head section under 3D waves becomes nearly 3.5 times the value of critical velocity for armour stone movement. In the case of 2D waves, the high velocities with higher occurrence frequencies than those of 3D waves appear in the back head section due to plunge of the strong current generated on the front and middle head sections.

Further numerical analysis of wave kinematics over the heads and trunks as a continuation of this study is expected to make the weight of stable armour units under 3D waves clear.

References

Isaacson, M. (1992), "Diffraction model of directional wave generation in a basin with partially reflecting boundaries", Report prepared for National Research Council of Canada.

Matsumi, Y., Mansard, E.P.D. and Rutledge, J. (1994), "Influence of wave directionality on stability of breakwater heads", Proc. 24th Int. Conf. on Coastal Engineering, ASCE, 1397-1411.

Matsumi, Y., Kimura, A. and Ohno, K. (1996), "Velocity field measurements over breakwater heads under 3D waves", Proc. 25th Int. Conf. on Coastal Engineering, ASCE, 1776-1788.

Mitsuyasu, H. et al (1975), "Observation of the directional spectrum of ocean waves using a cloverleaf buoy", Jour. Physical Oceanography, Vol.5, 750-760.

Van der Meer, J.W. (1987), "Stability of breakwater armour layers - design formulae", Coastal Engineering, 219-239.

Goda, Y. (1985), Random seas and design of maritime structures, University of Tokyo Press, Japan.